PHYSICAL REVIEW D

PARTICLES AND FIELDS

THIRD SERIES, VOLUME 35, NUMBER 5 1 MARCH 1987

# Search for charmed mesons produced in hadronic interactions

G. Ginther,[a] R. M. Edelstein, C. P. Forsyth,[b] K. Gamarnik, A. E. Kreymer,[c] R. J. Lipton, J. M. McQuade,[d] D. M. Potter, J. S. Russ, and L. Spiegel[e]
*Carnegie-Mellon University, Pittsburgh, Pennsylvania 15213*

D. E. Johnson
*Fermilab, Batavia, Illinois 60510*

D. Buchholz, L. M. Cremaldi,[f] S. W. Delchamps,[c] H. S. Mao,[g] J. L. Rosen, W. Sakumoto,[a] R. A. Schluter, S. B. Sontz,[h] and C. Winter[i]
*Northwestern University, Evanston, Illinois 60201*

J. M. Bishop, N. N. Biswas, N. M. Cason, L. Dauwe,[j] J. Godfrey, V. P. Kenney, P. Mooney, R. Pemper,[k] E. Rojek, R. C. Ruchti, M. Sarmiento, and W. D. Shephard
*University of Notre Dame, Notre Dame, Indiana 46556*
(Received 17 March 1986)

The hadronic production of charmed states was studied in a two-arm spectrometer using a 205-GeV/$c$ negative-pion beam incident upon a beryllium target. One arm, filled with dense absorber, triggered the detectors upon the passage of a muon with a moderate transverse momentum and a total momentum of at least 4 GeV/$c$. The other arm was an open-geometry magnetic spectrometer which had both neutral- and charged-particle identification capabilities. The apparatus, the data, and an invariant-mass-plot search for evidence of charmed-meson production through several charged-particle decay modes are described. The $K\pi$, $K\pi\pi$, and $K\pi\pi\pi$ mass plots fail to reveal significant $D$-meson signals. Based upon the $K\pi$ mass plots, the 95%-confidence upper limit on the $D\bar{D}$ production cross section is found to be less than 51 $\mu$b per nucleon for the production models tested. A search for evidence of charged-$D^*$ production yields $30\pm16$ combinations above background in association with the expected trigger muon charge. Interpreted as a $D^*$ signal, this excess corresponds to a model-dependent inclusive $D\bar{D}$ production cross section of $34\pm18^{+14}_{-9}$ $\mu$b per nucleon. Model-dependent upper limits on the ratio of the $F$ to $D$ cross sections are also presented.

## I. INTRODUCTION

Considerable experimental effort has been expended in the study of the hadronic production of charmed particles.[1] Even though the absolute rate of charmed-particle production in fixed-target experiments is relatively high, small individual branching ratios, large multiplicities, and enormous backgrounds have made the extraction of information on the hadronic production of charmed particles difficult.

Because of the short lifetime of charmed weak decays and their relatively large semileptonic branching ratios, charmed particles are an important source of prompt leptons. Fermilab experiment E515 was a study of 205-GeV/$c$ $\pi^-$-beryllium interactions selected with a prompt-muon trigger. The data were accumulated with a two-arm spectrometer. The trigger arm, which was filled with dense absorber, triggered the detector upon the passage of a muon with moderate transverse momentum and a momentum of at least 4 GeV/$c$. The beam, target, and absorber geometry were designed to discriminate in favor of muons of prompt origin. The forward arm was an open-geometry magnetic spectrometer which contained both neutral- and charged-particle identification capabilities. The experiment was designed to trigger on prompt muons, some of which arise from charmed-(anticharmed-) particle decays, and then observe the decay products of the associatively produced anticharmed (charmed) state in the forward arm. Studies of coincidences between muons in the trigger arm and leptons in

 

the forward arm have been presented previously, and an excess of opposite-sign $\mu e$ pairs was observed which corresponded to a model-dependent $D\bar{D}$ cross section of $11 \pm 4$ $\mu$b (Ref. 2). An investigation of $K^{\mp}\pi^{\pm}$, $K^{\mp}\pi^{\pm}\pi^{\pm}$, $K^{\mp}\pi^{\pm}\pi^{\mp}\pi^{\pm}$, and $K^{\pm}K^{\mp}\pi^{\pm}$ invariant-mass plots in search of evidence of the hadronic production of charmed mesons is presented here. Model-dependent upper limits on the $D\bar{D}$ cross section are determined from the $K^{\mp}\pi^{\pm}$ mass plot. A $D\bar{D}$ cross-section measurement determined from a charged-$D^*$ search is also presented. Upper limits on the ratio of the $F$ to $D$ cross sections are extracted from a $\phi\pi^{\pm}$ mass plot combined with the results of the charged $D^*$ search.

The spectrometer and the data are described in Sec. II. Section III describes the event reconstruction. Section IV summarizes the invariant-mass-plot search. The Monte Carlo simulation is described in Sec. V. The cross-section calculations and conclusions are presented in Sec. VI.

## II. APPARATUS

### A. Beam system

The spectrometer was in the Fermilab M1 West beam line 500 m downstream of the Meson Center target. The beam line transported a negatively charged unseparated beam with a mean momentum of 205 GeV/$c$. Although the incident beam particles were not identified, the noninteracting beam was 96% $\pi^-$, 3.5% $K^-$, and 0.5% $\bar{p}$ (Ref. 3).

The beam was focused to a vertical height ($Y$) of 1 mm at the target. This narrow beam minimized the vertical distance between the interaction point in the target and the absorber in the trigger arm. Immediately upstream of the target were two scintillation counters, $B1$ and $B2$, which were overlapped by 1.5 mm in $Y$ (Fig. 1). The beryllium target was 2 mm high and 30 mm long. The top of the target was 1 mm below the lowest edge of the trigger-arm absorber.

The beam was several centimeters wide ($X$) at the target. The $X$ position of the beam particles was determined by three proportional wire chambers (PWC's), which had 24 anode wires per inch. Two additional scintillation counters upstream of the target served as an upstream interaction veto. A wall of scintillation counters (1 m wide and 0.5 m high) shadowed most of the trigger arm, and this antiwall vetoed most events containing halo muons incident upon the trigger arm.

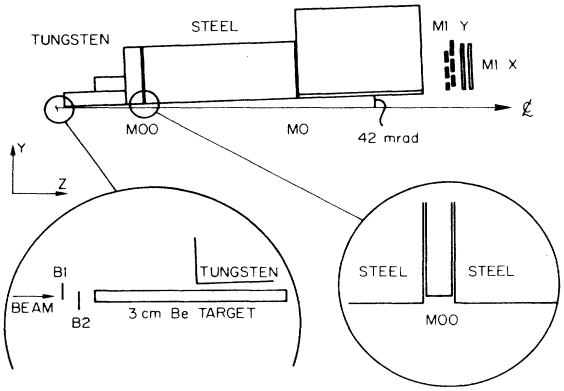


FIG. 1. Elevation view of the beryllium target and upstream trigger-arm absorber geometry.

### B. Trigger arm

The spectrometer is illustrated in Fig. 2. It was divided into two relatively independent detector systems referred to as the trigger arm and the forward arm. The trigger arm was composed of those detectors above a plane inclined at 42 mrad from the horizontal and passing through the target. The trigger arm subtended $\pm 150$ mrad horizontally and $+42$ mrad to $+170$ mrad vertically. It consisted of tungsten and steel absorber, scintillation counters, the yoke of the spectrometer magnet, and PWC's.

The absorber was placed as close as feasible to the target so as to discriminate in favor of muons of prompt origin by increasing the probability that charged pions and kaons interacted hadronically before they could decay semileptonically. The first 0.15 m of absorber was tungsten. The remaining 0.76 m of absorber upstream of the spectrometer magnet was steel. Two scintillation counters, $M00$ and $M0$, were sandwiched in the steel.

The next detector in the trigger arm was the scintillation-counter hodoscope $M1$, which was divided into left and right halves. Each half contained seven $X$ counters and six $Y$ counters. The individual counters were overlapped to achieve an effective angular resolution of 10 mrad.

The 1.22-m-long return yoke of the spectrometer magnet served as additional absorber as well as a charge and momentum analyzer for particles passing through the trigger arm. The $M2$ scintillation counter hodoscope consisted of four counters positioned between the downstream end of the magnet yoke and the magnet's saddle coil.

The next six elements of the trigger arm were PWC's; three of the PWC's measured $X$ coordinates, while two others recorded $Y$ coordinates, and one had its sense-wire plane inclined at 16° with respect to vertical and measured rotated coordinates. After the PWC's was another 0.4 m of steel, referred to as the downstream trigger-arm ab-

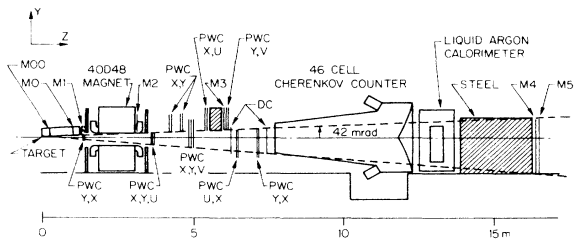


FIG. 2. Elevation view of the E515 spectrometer, showing both the trigger and forward arms. The trigger arm includes those elements above a place inclined at 42 mrad from the horizontal. $M00$, $M0$, $M1$, $M2$, and $M3$ were scintillation counters employed in the prompt-muon trigger.

sorber. The $M3$ hodoscope, which consisted of six scintillation counters, was located just beyond that absorber. Two additional PWC's recorded $Y$ coordinates and rotated coordinates.

All eight trigger arm PWC's were of the same basic design. The anode plane of each PWC had a 3-mm pitch but pairs of adjacent wires were shorted together, resulting in an effective 6-mm sense wire spacing.[4]

### C. Trigger logic

The signals BEAM and M were the primary components of the prompt muon trigger. BEAM indicated the presence of a beam particle in the target unaccompanied by beam halo, while M was a coincidence consistent with the passage of a muon through the trigger arm.

The signal BEAM was generated by a coincidence in the beam counters $B1$ and $B2$ combined with the absence of signals from the antiwall and the upstream interaction counters.

The signal M1 was generated by a coincidence between signals from $X$ and $Y$ counters in the same half of the $M1$ hodoscope. A coincidence between a signal from an $M2$ hodoscope element and any of the three nearest $M3$ hodoscope elements generated a signal called MX. Triggering particles which satisfied the MX requirement had $XZ$ slopes downstream of the spectrometer magnet of between $\pm 0.250$. The signal M was a coincidence of the signals M00, M0, M1, and MX, where M00 and M0 were the signals from the counters $M00$ and $M0$, respectively. M was interpreted as evidence of the passage of a muon through the trigger arm because a signal particle generating the necessary signals must have traversed at least 2.4 m of steel.

The prompt-muon trigger was defined by a coincidence between the signals BEAM and M and BEAMGATE in the absence of a dead-time signal, where BEAMGATE was the accelerator signal that indicated a beam spill in progress.

### D. Forward arm

The forward arm subtended $\pm 200$ mrad horizontally, and $-80$ mrad to $+42$ mrad vertically. The forward arm contained a large aperture dipole magnet, PWC's, drift chambers (DC's), a large multicell Cherenkov counter, a large lead—liquid-argon electromagnetic calorimeter (LAC), and a forward muon identifier.

The 40D48 spectrometer magnet had a brass insert on the upper pole face to provide absorber above the 42-mrad plane between the forward arm and the trigger arm. A helium filled polyethylene bag occupied the magnet aperture. A 2400-A current generated a 18.6-kG central field in the $-Y$ direction. The field provided a 0.80-GeV/$c$ transverse-momentum impulse.

There were two forward-arm PWC's upstream of the magnet, one measuring $X$ coordinates (UPMX), and the other measuring $Y$ coordinates (UPMY). Downstream of the magnet were four $X$ PWC's, three $Y$ PWC's, and three PWC's whose sense planes were rotated by $\pm 14°$ from the vertical. The UPMX, UPMY, and a downstream magnet $Y$ PWC had 24 anode wires per inch; the remainder of the forward arm PWC's had 12 anode wires per inch.[5] Three different readout systems were employed to instrument the 9000 sense wires of the forward-arm PWC's. The highest-rate system was deployed in the central regions of the forward-arm PWC's. The outer portions of most of the PWC's were instrumented with a lower-rate readout system.[6] A shift-register readout system was employed in regions of one downstream $X$ and one downstream $Y$ PWC.

Two drift chambers (DC's) were located downstream of the magnet and measured $X$ coordinates. Each DC had 96 sense wires with a 2-cm wire spacing. The DC gas was a mixture of equal parts of argon and ethane. This system had a hit rate limitation of about 4 MHz on any individual wire.

A large threshold Cherenkov counter filled with nitrogen gas at atmospheric pressure was located downstream of the last DC. The threshold momentum for the generation of Cherenkov radiation was 0.02 GeV/$c$ for electrons, 4.3 GeV/$c$ for muons, 5.7 GeV/$c$ for pions, 20.2 GeV/$c$ for kaons, and 38.3 GeV/$c$ for protons. The Cherenkov counter contained 4.3 m of radiator and had 24 cells above and 22 cells below the beam center line. Each cell consisted of a five-inch-diameter RCA 4522 photomultiplier tube mounted in a 15-cm-wide aluminized cone that faced a cylindrical mirror. The upper and lower halves of the counter were effectively decoupled by a 10-cm-wide nonreflective slot in the mirrored surfaces. A hole was cut into the center mirrors to avoid collecting Cherenkov light from the noninteracting beam particles.

The LAC, which was located downstream of the Cherenkov counter, contained 26 radiation lengths and 1.2 pion absorption lengths. Details on the construction and performance of the LAC are available elsewhere.[7]

The forward-arm muon identifier was composed of 2.9 m of steel followed by the $M4$ and $M5$ hodoscopes. The $M4$ hodoscope was an array of proportional tubes arranged to measure the $Y$ coordinates of charged particles. The $M5$ hodoscope was a set of 18 scintillation counters that measured $X$ coordinates. A 20-cm by 20-cm hole in the steel allowed the noninteracting beam to pass through the spectrometer.

### E. Data

A total of $1.9\times 10^6$ prompt-muon triggers were recorded during the data run. The average BEAM per one-second spill was $4.8\times 10^6$. The incident beam was well centered upon the $B1$ and $B2$ overlap and 83% contained within the overlap. The mean number of M signals per live BEAM was $4.9\times 10^{-5}$. The mean number of prompt muon triggers per live BEAM was $6.6\times 10^{-6}$. The fractional live time of the spectrometer was 68%. Including corrections for the estimated multiple occupancy of the rf buckets (1.05), the attenuation of the beam in the target (0.97), and the damaged or missing scaler records (1.07), the total number of incident live beam particles employed in this study is $2.95\times 10^{11}$.

## III. EVENT RECONSTRUCTION

### A. Interaction location

The $Y$ and $Z$ positions of the interaction in the target were taken to be target center. The $X$ location of the interaction was determined from the hits in the beam PWC's. Because there was frequently more than one vertex candidate in an event, a cut was implemented, referred to as the clean vertex cut, that excluded most events with ambiguous interaction locations.[8]

About 69% of the events survived the clean vertex cut. It is estimated that 96% of the events that survived the clean vertex cut had their vertex position properly identified.

### B. Trigger-arm track finding

The eight trigger-arm PWC's were employed to find straight-line tracks downstream of the spectrometer magnet. About 42% of the prompt-muon-triggered events had at least one downstream trigger-arm track defined by two or three hits from among the three $X$ PWC's, two or three hits from among the three $Y$ PWC's, and one or two rotated hits consistent with the combination of the $XZ$ and $YZ$ line segments.

The interaction location and each pair of $X$ and $Y$ hits from the same half of the $M1$ hodoscope determined straight lines upstream of the magnet which were extrapolated to the spectrometer-magnet midplane. Each downstream trigger-arm track was also extrapolated to the magnetic midplane. The $M1$ point and downstream track that yielded the smallest position deviation at the magnetic midplane were assumed to be associated. The track's momentum was calculated by an iterative fit that took into account multiple scattering and energy loss.

A trigger-arm track was considered a muon if it satisfied all of the following requirements.

(1) If the track passed through $M2$ and $M3$ hodoscope elements, those elements must be latched.

(2) The track must have at least one rotated hit within a more restrictive search window.

(3) The track must employ a hit in at least one of the two PWC's beyond the downstream trigger-arm absorber.

(4) The difference between the extrapolated upstream and downstream track positions at the magnet midplane must be within $\pm 0.25$ m in both $X$ and $Y$. Approximately 64% of the DST events had at least one trigger-arm track identified as a muon by the above critieria. (A DST event is a prompt-muon-triggered event that satisfied the clean vertex cut and had at least one trigger-arm track.) The mean number of trigger-arm muons was 0.8 per DST event.

To contribute to the charm search mass plots, at least one of the trigger-arm muons in an event must also satisfy all of the following requirements.

(1) The track must extrapolate through $M2$ and $M3$ hodoscope elements that are consistent with a triggering road MX.

(2) If the muon has positive charge, its momentum must be $\leq 50$ GeV/$c$.

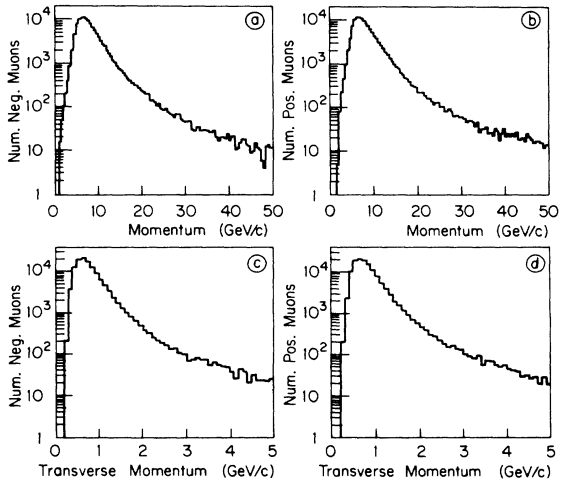


FIG. 3. Trigger-arm muon distributions. (a) Momentum distribution of the negative triggering muons. (b) Momentum distribution of the positive triggering muons. (c) Transverse-momentum distribution of the negative triggering muons. (d) Transverse-momentum distribution of the positive triggering muons. (Events with more than one triggering muon are excluded from the momentum distribution plots.)

(3) The muon must not be a halo muon. (A halo muon with a muon with downstream $XZ$ slope between $-0.012$ and $+0.010$ and downstream $YZ$ slope $<0.015$.)

About 58% of the DST events had at least one such muon, which was referred to as a triggering muon.

Of the DST events with a triggering muon, 87% had only one such muon. The momentum and transverse-momentum distributions of those triggering muons are shown in Fig. 3. There were about 6.7% more positive signal triggering muons than negative single triggering muons.

### C. Forward-arm track finding

Those events that had at least one trigger-arm track were subjected to a search for forward-arm tracks. Although the $XZ$ plane was the bend plane of the magnet, some tracks with momenta below 7 GeV/$c$ deviate measurably from straight lines in the $YZ$ view due to the fringe fields of the magnet and due to the change in the $Z$ component of the momentum. A simple thin lens model was employed to account for these deviations so that the search for $YZ$ segments could employ both the upstream and downstream $Y$ PWC's.

The forward-arm tracks have a minimum of four hits from among the six downstream $X$ chambers, two hits from the four $Y$ PWC's, and at least one hit from the three rotated PWC's. These minimal hit requirements admitted tracks of questionable quality. When the track quality cut was invoked, it eliminated every track that satisfied any of the following conditions.

(1) The track had one rotated hit and one downstream $Y$ hit.

(2) The track had one rotated hit, four $X$ hits, and no match up in UPMX.

(3) The track had two rotated hits, one downstream $Y$ hit, four $X$ hits, but no matchup in UPMX.

This cut rejected approximately 12% of the forward-arm tracks. The mean number of forward-arm tracks that survived the track quality cut was 5.9 per event.

### D. Forward-arm particle-identification analysis

Kaon quality factors $Q_{K1}$ and $Q_{K2}$ were calculated for each charged track. They represent how well the Cherenkov information associated with this event matched the hypothesis that the track was generated by a kaon relative to how well it matched either the kaon or the pion hypothesis for that track's identity. The kaon quality factors range from zero to one with larger values corresponding to greater likelihood that the track was generated by a kaon.

96% of all forward-arm tracks with momenta between 7 and 20 GeV/$c$ intersected the active area of the Cherenkov counter, and 70% of those were isolated, while 22% were members of groups of two, and the remaining 8% were members of groups that contained three or more tracks. The calculation of the kaon quality factors took into account the contributions of other members of a group.

During the calculation of $Q_{K1}$, all signals below 0.4 photoelectrons were neglected, while $Q_{K2}$ calculations had a threshold of 1.0 photoelectron. Consequently, $Q_{K1}$ identified pions with higher efficiency than $Q_{K2}$. However, $Q_{K1}$ also misidentified kaons more frequently than $Q_{K2}$.

### E. Standard states

The spectrometer's capabilities are illustrated by mass plots which show clear evidence of noncharmed-particle decays. Figure 4 shows a $K^+K^-$ invariant-mass plot. Only forward-arm tracks that satisfy the track quality cut and have momenta between 7 and 20 GeV/$c$ and have $Q_{K2} \geq 0.7$ were identified as kaons. (Cherenkov efficiency studies indicate that 76% of the kaons with momenta between 7 and 20 GeV/$c$ have $Q_{K2} \geq 0.7$ and only 4% of the pions in that momentum range have $Q_{K2} \geq 0.7$.) A clear and significant $\phi$ mass peak is observed. The $K^+K^-$ mass plot was fit to a Gaussian plus a fourth-order polynomial. The mean of the Gaussian is at $1.0201 \pm 0.0005$ GeV/$c^2$, and the standard deviation is $0.0039 \pm 0.0006$ GeV/$c^2$; the mean mass and the measured width of the peak are consistent with Monte Carlo expectations for the $\phi$ meson.

A mass plot of opposite-sign $K\pi$ pairs (Fig. 5) exhibits evidence of the neutral $K^*(890)$. The track quality cut has been imposed. The mass assignment scheme for this $K\pi$ plot is as follows. If an isolated track was in the discrimination domain of the Cherenkov,[9] and had $Q_{K2} < 0.1$, then that track was assigned a pion mass only. If an isolated track within the discrimination domain had $Q_{K1} \geq 0.8$, then that track was assigned a kaon mass only. All other tracks were assigned both identities. Consequently, only combinations which were consistent with the Cherenkov-counter data contribute to the mass plot. An isolated pion in the discrimination domain had a 91% probability of being identified only as a pion by this scheme, and a $<1\%$ probability of being identified only as a kaon. An isolated kaon in the discrimination domain had a 69% probability of being identified only as a kaon, and a 9% probability of being identified only as a pion.

Because of the prompt-muon trigger employed in accumulating this data, the calculation of inclusive $\phi$ and $K^*$ cross sections are compromised; nevertheless when simple assumptions are made, the observed peaks correspond to cross sections which are within an order of magnitude of the expected values.

The data gathered by the LAC revealed $\pi^0$ and $\eta$ signals in the two photon mass plots. The neutral pions were combined with the charged pions to yield evidence for the $\pi^+\pi^-\pi^0$ decay mode of the $\omega(783)$, and the two-pion decay mode of the $\rho^-$ (Ref. 10).

## IV. THE CHARM SEARCH

Assuming that the triggering muon originated from the associated production of a charm-anticharm quark pair followed by the semileptonic decay of the charmed or anticharmed state, the charge of the triggering muon con-

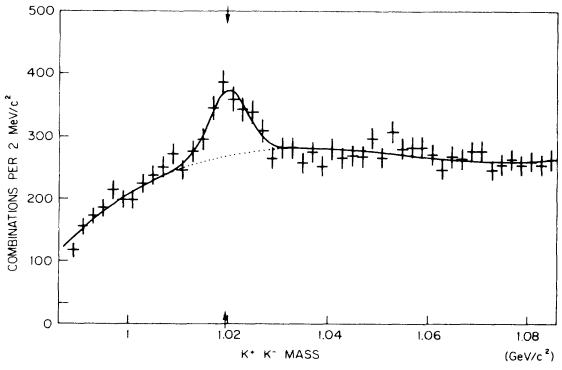


FIG. 4. Invariant-mass plots of oppositely charged pairs of tracks identified as kaons. Evidence of $\phi$ production is clear.

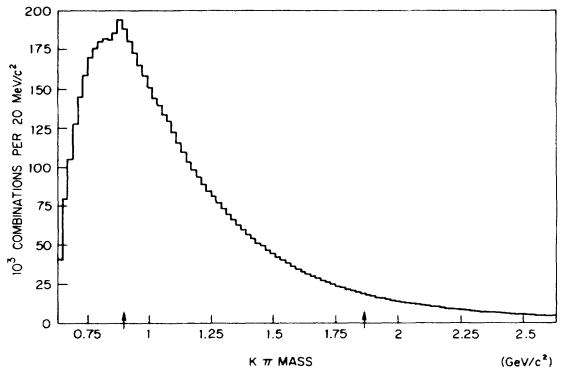


FIG. 5. $K^{\pm}\pi^{\mp}$ invariant-mass plot. Note the $K^*(890)$ peak.

strains the identity of the particles in the decay products of the partner state (in the absence of $D^0\overline{D}^0$ mixing).[11] For instance, when a neutral $D$ meson decays into a charged kaon and one or three charged pions, the sign of the kaon should be the same as the sign of the triggering muon. For a charged $D$ or $D^*$ meson decaying into a charged kaon and two charged pions, the sign of the kaon should be the same as the triggering muon sign and opposite of the charged $D$ or $D^*$ parent state. This correlation between the triggering muon sign and the kaon charge allows a separation of the mass plots into "right-sign" and "wrong sign" plots.

To contribute to the charm-search mass plots presented here, an event must satisfy the clean vertex cut and have at least one triggering muon. (Only 24% of the prompt-muon triggers had at least one reconstructed triggering muon, and the efficiency of the muon reconstruction was 93%.) To take advantage of the right-sign and wrong-sign classification of the mass plots, an event was employed in the charm search only when all muons in the trigger arm had the same sign (excluding halo muons and positive muons with momenta $>50$ GeV/$c$). This requirement eliminated 1.2% of the DST events that had at least one triggering muon. Of the $2.9\times10^5$ events employed in this charm search, 51.67% had positively charged triggering muons. Thus there was a small but statistically significant trigger charge asymmetry in this data sample.

### A. $K\pi$ invariant-mass plots

The broken line histogram in Fig. 6 is an invariant-mass plot of all right-sign $K^+\pi^-$ and $K^-\pi^+$ combinations with the particles identified by the consistent Cherenkov scheme employed in the $K^*$ mass plot. The track quality cut has been imposed. There is no significant enhancement in the vicinity of the neutral-$D$-meson mass.

The inset in Fig. 6 shows the distribution of the cosine of $\theta_{\text{c.m.}}$ for those right-sign $K\pi$ pairs that have mass between 1.815 and 1.915 GeV/$c^2$. $\theta_{\text{c.m.}}$ is the angle between the direction of the kaon in the $K\pi$ center-of-momentum frame and the direction of the $K\pi$ pair in the laboratory. This $\cos(\theta_{\text{c.m.}})$ plot shows that many of the high-mass combinations arise from pairs that include a very forward or very backward kaon. Since the $D$ is a pseudoscalar meson, the $\cos(\theta_{\text{c.m.}})$ distribution for kaons from the $K\pi$ decays of neutral $D$ mesons should be uniform. Furthermore, the acceptance of the spectrometer for $D\to K\pi$ introduced greater losses for those $K\pi$ pairs that had large forward or backward kaon angles. The lower histogram in Fig. 6 shows the right-sign $K\pi$ mass plot with the requirement that $-0.7\le\cos(\theta_{\text{c.m.}})<0.7$. Although no signal is observed, this cut reduces the upper limits that can be extracted from the data.

The number of combinations above background in the vicinity of the $D$ meson mass in the right-sign $K\pi$ mass plot with the $\cos(\theta_{\text{c.m.}})$ cut was determined by fitting a fourth-order polynomial to the mass plot, excluding the contributions between 1.795 and 1.935 GeV/$c^2$. The resulting curve, which had a $\chi^2$ per DF of 35/48, is also

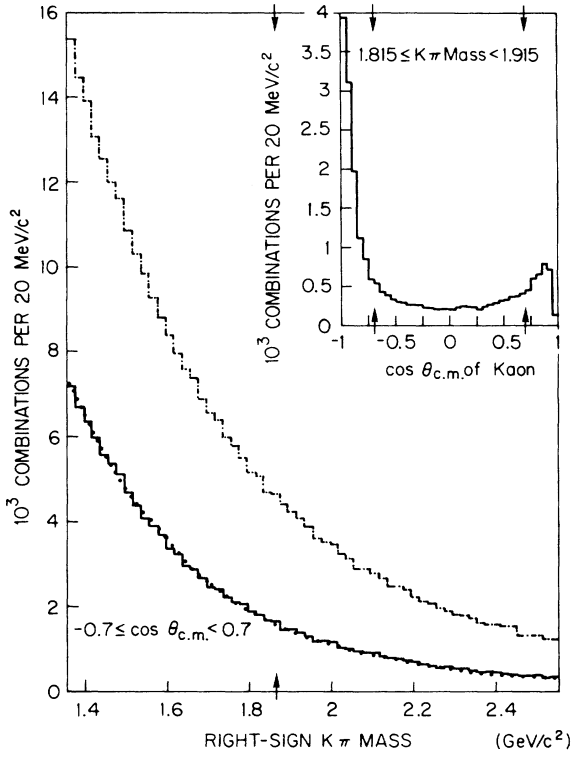


FIG. 6. Right-sign $K\pi$ invariant-mass-plot without (broken line) and with (continuous line) a cut applied on $\cos(\theta_{\text{c.m.}})$. $\theta_{\text{c.m.}}$ is the angle between the kaon in the center-of-momentum frame of the $K\pi$ system and the $K\pi$ direction in the laboratory. The inset shows the $\cos(\theta_{\text{c.m.}})$ distribution for those $K\pi$ combinations with mass in the range of 1.815 to 1.915 GeV/$c^2$.

shown in Fig. 6. The number of combinations above background with masses between 1.815 and 1.915 GeV/$c^2$ is $104\pm105$ (Ref. 12).

In this analysis, additional cuts on the triggering muons and on various kinematic variables associated with the $K\pi$ pairs failed to reveal any statistically significant peaks in the $K\pi$ mass plots in the region of the neutral-$D$ mass.

### B. $K\pi\pi\pi$ and $K\pi\pi$ invariant-mass plots

A search for evidence of the $K^-\pi^+\pi^-\pi^+$ and $K^+\pi^-\pi^+\pi^-$ decay modes of the neutral $D$ mesons was also performed. Although this decay mode has a larger branching ratio than the $K\pi$ decay mode, the background for the $K\pi\pi\pi$ decay mode peaked near the expected signal location. Furthermore, the larger combinatorial backgrounds and lower acceptances made the four-body final state less sensitive than the $K\pi$ decay mode.

Similar searches of right-sign $K^-\pi^+\pi^+$ and $K^+\pi^-\pi^-$ mass plots failed to reveal statistically significant evidence of charged-$D$ production. Once again, the larger combinatorial background and smaller acceptance make this decay mode less sensitive to charm production than the $K\pi$ decay mode.

### C. Charged-$D^*$ search

The mass difference between the charged $D^*$ and the neutral $D$ is only slightly larger than the charged-pion mass. As a result, the charged $D^*$ has a relatively narrow width, and the resolution of the mass difference between the $D^*$ and the $D$ is much better than the mass resolution for the $D^*$. The restrictive kinematics of the charged-$D^*$ decay provides substantial background suppression.

Figure 7(a) shows a plot of the mass difference between the right-sign $K\pi\pi$ combinations and the $K\pi$ subsets with the $K\pi$ mass restricted to between 1.815 and 1.915 GeV/$c^2$ (Ref. 13). An enhancement is observed near 0.1465 GeV/$c^2$. To maximize acceptance, Cherenkov identification was not employed in this plot. Figure 7(b) shows the right-sign $K\pi$ mass plot with the difference between the $K\pi\pi$ and the $K\pi$ mass restricted to between 0.145 and 0.148 GeV/$c^2$, which is the region of the observed enhancement in the mass difference plot. That right-sign $K\pi$ mass plot exhibits an enhancement in the vicinity of the neutral-$D$-meson mass.

The background curve shown in Fig. 7(a) is a fourth-order polynomial resulting from a fit excluding contributions between 0.1445 and 0.1485 GeV/$c^2$. The fit had a $\chi^2$ per DF of 20/26. There is an excess of $26\pm16$ combinations above background with a mass difference between 0.145 and 0.148 GeV/$c^2$. The mean of the mass difference between the $D^{*\pm}$ and the neutral $D$ reported in other experiments is about 1 MeV/$c^2$ below the center of the observed excess, which is within expectations for a signal from $D^*$ decay. The fourth-order polynomial background curve shown in Fig. 7(b) resulted from a fit excluding mass combinations between 1.795 and 1.935 GeV/$c^2$. The $\chi^2$ per DF of the fit was 50/47. There is an excess of $33\pm14$ combinations between 1.815 and 1.915 GeV/$c^2$ in this right-sign $K\pi$ mass plot.

Figure 8 contains the corresponding mass difference plot and $K\pi$ mass plot with the wrong-sign trigger muon correlations. Using the same fitting procedure as for the right-sign mass plots, the wrong-sign mass difference plot has an excess of $-4\pm15$ combinations between 0.145 and 0.148 GeV/$c^2$ ($\chi^2$/DF=15/26); the wrong-sign $K\pi$ mass plot has an excess of $6\pm12$ combinations between 1.815 and 1.915 GeV/$c^2$ ($\chi^2$/DF=56/47).

Although the enhancements in the right-sign $K\pi$ mass plot and mass difference plot are small, they are of comparable size and appear in both plots with minimal software cuts. The 153 combinations within the band containing the enhancement came from 150 different events from runs spread throughout the data sample. When the right-sign $K\pi$ mass plot is fit to a Gaussian-plus-polynomial background, the mean of the Gaussian is $1.847\pm0.010$ GeV/$c^2$ and the standard deviation is $0.022\pm0.010$ GeV/$c^2$. Thus, the locations of the $K\pi$ and mass difference enhancements are both consistent with those anticipated for evidence of charged $D^*$ decays. The widths of the enhancements are also comparable to those anticipated from Monte Carlo studies. In addition, no similar enhancement is observed in the corresponding wrong-sign plots. Thus the interpretation of this small excess as evidence of charged-$D^*$ production is consistent with the available information.

### D. $\phi\pi$ invariant-mass plot

The $\phi\pi^{\pm}$ decay mode of the $F$ meson has been observed in several $e^+e^-$ experiments.[14–16] Evidence for the ha-

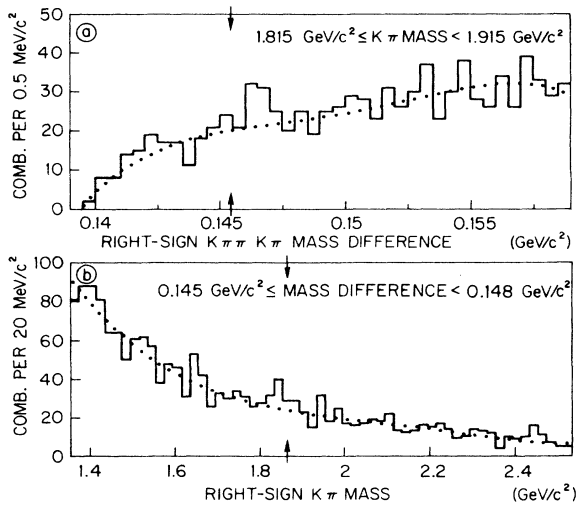


FIG. 7. Right-sign charged-$D^*$ search. (a) Right-sign plot of the mass difference between the $K\pi\pi$ and the $K\pi$ with the $K\pi$ mass restricted to the range 1.815 to 1.915 GeV/$c^2$. (b) Right-sign $K\pi$ mass plot with the difference between the $K\pi\pi$ and the $K\pi$ mass restricted to the range 0.145 through 0.148 GeV/$c^2$.

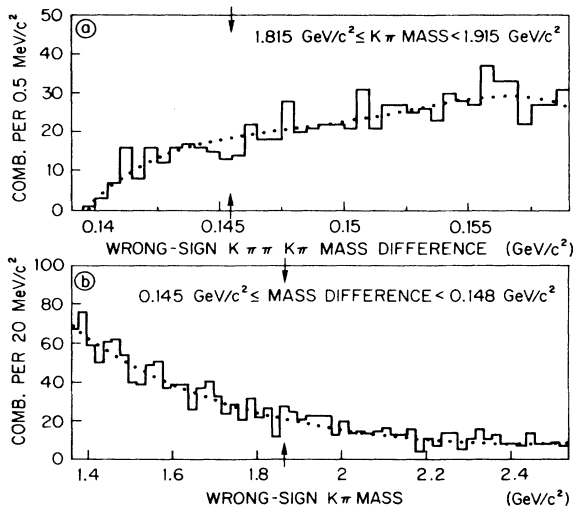


FIG. 8. Wrong-sign charged-$D^*$ search. (a) Wrong-sign plot of the mass difference between the $K\pi\pi$ and the $K\pi$ with the $K\pi$ mass restricted to the range 1.815 to 1.915 GeV/$c^2$. (b) Wrong-sign $K\pi$ mass plot with the difference between the $K\pi\pi$ and the $K\pi$ mass restricted to the range 0.145 through 0.148 GeV/$c^2$.

dronic production of $F$ mesons is quite scarce, although a few events have been reported.[17] Figure 9 shows the invariant-mass plot of the right-sign $K^+K^-\pi^\pm$ combinations where tracks between 7 and 20 GeV/$c$ with $Q_{K2} \geq 0.7$ are identified as kaons and all other tracks are considered pions. Only those combinations that have a $K^+K^-$ mass in the range 1.012 to 1.028 GeV/$c^2$ contribute to this mass plot. The track quality cut has been imposed. There is no statistically significant signal in the vicinity of the $F$ mass (1.97 GeV/$c^2$).

The number of combinations above background in the vicinity of the $F$ mass was determined by fitting a fourth-order polynomial to the mass plot excluding contributions between 1.915 and 2.035 GeV/$c^2$. The $\chi^2$ per DF was 59/53 and there were $17 \pm 16$ combinations above background with masses between 1.925 and 2.925 GeV/$c^2$.

## V. SPECTROMETER SIMULATION

Both the resolution and the acceptance of the spectrometer was studied by Monte Carlo simulation. The trigger-arm momentum resolution is

$$[(\delta p/p)_{\text{trig}}]^2 \approx (0.15)^2 + (0.013p)^2 ,$$

where $p$ is in GeV/$c$. The sign of the reconstructed simulated muon was nearly always the same as the sign of the generated muon. The trigger-arm track-finding program exhibited essentially no inefficiency in reconstructing simulated tracks that met the minimum requirements. When the effects of multiple scattering, chamber resolution, and efficiency are included, the forward-arm momentum resolution is

$$[(\delta p/p)_{\text{for}}]^2 \approx (0.0060)^2 + (0.000\,66p)^2 .$$

The forward-arm track-finding program was 97% efficient for tracks with momenta above 7 GeV/$c$, but the efficiency fell off slowly at lower momenta, due to the limitations of the simple thin lens model employed in the $YZ$ tracking.

Figure 10 illustrates the trigger-arm acceptance for muons from the semileptonic decay of $D$ mesons as a function of the Feynman $x$ ($x_F$) and transverse momentum ($p_T$) of the parent $D$ meson. The effects of chamber inefficiencies and the cuts employed to define triggering

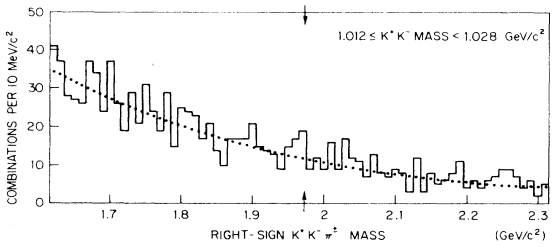


FIG. 9. Right-sign $K^+K^-\pi^\pm$ mass plot for the $F \to \phi\pi$. The $K^+K^-$ mass is restricted to the range 1.012 to 1.028 GeV/$c^2$.

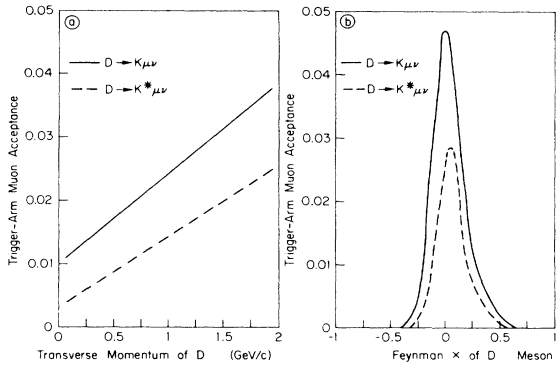


FIG. 10. Trigger-arm acceptance for muons from the semileptonic decay of $D$ mesons. (a) Acceptance as a function of $p_T$ using the uncorrelated model with $n=3$. (b) Acceptance as a function of $x_F$ using the uncorrelated model with $b=1.1$ (GeV/$c$)$^{-2}$.

muons are included. The imposition of the trigger-arm PWC efficiencies accounted for a 6% reduction in the muon acceptance, while the other cuts reduced the acceptance by 1%. The trigger-arm muon acceptances were independent of the muon sign for the models tested.

The forward-arm acceptance for the decay $D \to K^\mp\pi^\pm$ is illustrated in Fig. 11. That figure also shows the forward-arm acceptance for the $D^{*\pm}$ decay into a charged pion and a neutral $D \to K^\mp\pi^\pm$. The forward-arm acceptances are essentially equal for the charmed particle and corresponding antiparticle states. The chamber efficiencies and the minimum hit requirements result in a 75% efficiency for finding a forward-arm track that was geometrically accepted by the forward arm. 2% of the simulated particles undergo secondary interactions in the target. 6% of the simulated forward-arm kaons and 1% of the simulated pions decayed before getting through the last drift chamber.

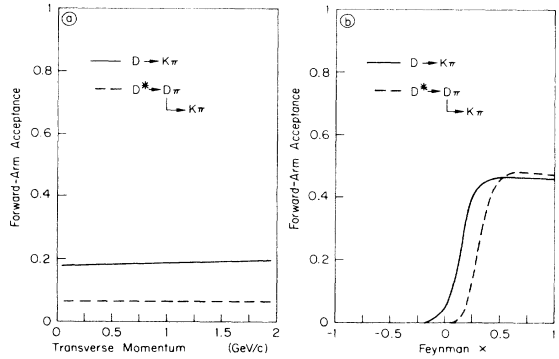


FIG. 11. Forward-arm acceptance for the decay $D \to K^\mp\pi^\pm$ and $D^{*\pm} \to D\pi^\pm$. (a) Acceptance as a function of $p_T$ using the uncorrelated model with $n=3$. (b) Acceptance as a function of $x_F$ using the uncorrelated model with $b=1.1$ (GeV/$c$)$^{-2}$.

The acceptance of the trigger arm clearly favors $D$ mesons with $x_F$ around zero while the forward arm favors $D$ mesons with more positive $x_F$ values. Consequently, the cross-section results obtained in this experiment are dependent upon the kinematic correlations between the triggering particle and the state observed in the forward arm.

Two different types of models were employed in the calculation of the spectrometer acceptance for charmed states. The uncorrelated-production model generated an individual charmed particle selected from the distribution

$$\frac{d\sigma}{dx_F dp_T{}^2} \propto (1-|x_F|)^n \exp(-bp_T{}^2) .$$

The correlated-producted model generated a charmed-anticharmed pair with mass $M$, with the distribution

$$\frac{d\sigma}{dM\,dx_F dp_T{}^2} \propto \exp(-5M)(1-|x_F|)^n \exp(-bp_T) .$$

Then the pair decayed isotropically into charmed and anticharmed mesons. Note that the correlated model yields a significantly softer $x_F$ distribution for the individual charmed particles than the uncorrelated model for the same value of $n$.

## VI. RESULTS AND CONCLUSIONS

Cross sections are estimated based upon the following assumptions. The mass-number ($A$) dependence is linear.[18] The prompt-muon triggers which arose from the decay of charmed particles were all assumed to come from the decay of $D$ mesons.[19]

Since the $D$ and $D^*$ mesons have comparable masses, and assuming that the probabilities for a naked charm quark to dress itself with an up or a down quark are equal, then counting the spin degrees of freedom, the relative production ratios of direct $D$ and $D^*$ mesons is taken to be

$$D^0{:}D^+{:}D^{*0}{:}D^{*+} = 1{:}1{:}3{:}3 .$$

The same spin-weighted production ratios are assumed to apply to the antiparticles. Combining the above production ratios and the $D^*$ branching ratios, the $D^*$ decays are expected to be responsible for 82% of the neutral-$D$ mesons and 61% of the charged-$D$ mesons, and the ratio of the number of $D^0$ to $D^+$ is 2.16 after $D^*$ decay. Experiment NA27 reports that the $D^*$ cross sections are consistent with saturating the neutral-$D$ production and responsible for $48\pm27\%$ of the charged-$D$ production. Furthermore, assuming symmetry about $x_F$ of zero, the cross sections reported by NA27 yield a ratio of $D^0$ to $D^+$ of $1.8\pm0.6$ (Ref. 20). These NA27 results are consistent with the spin-weighted production ratio assumption. Assuming the inclusive muonic $D$ branching ratios are equal to the measured inclusive electronic $D$ branching ratios, and using the spin-weighted $D$ and $D^*$ production ratios, the average inclusive branching ratio for $D$ mesons into muons is

$$B_T = 0.683B(D^0 \to \mu^+ X) + 0.317B(D^+ \to \mu^+ X)$$
$$= 0.105 .$$

The spectrometer acceptance for a $D\bar{D}$ pair was calculated with the Monte Carlo simulation outlined in Sec. V. The trigger-arm acceptance was calculated by assuming that half the $D$ mesons whose decay products include a muon decay via the mode $D \to K\mu\nu$, while the other half decay via the mode $D \to K^*(890)\mu\nu$ (Ref. 21). The calculated acceptances must be corrected by a factor ($f$) which accounts for the fraction of events that are rejected by cuts not represented in the Monte Carlo simulation (primarily the clean vertex cut). Table I contains a compilation of the constants employed in the cross-section estimates.

### A. Upper limits from the $K\pi$ mass plots

The right-sign $K^-\pi^+$ and $K^+\pi^-$ mass plots can each be employed to measure the $D\bar{D}$ cross section independently; however, since the acceptances and backgrounds are similar for $K^-\pi^+$ and the $K^+\pi^-$ plots, the lowest upper limits are achieved by combining both right-sign mass plots, and thus increasing the acceptance by a factor

TABLE I. Constants employed in the cross-section calculations.

| | | |
|---|---|---|
| $N_b$ | Number of incident live beam | $2.95\times10^{11}$ |
| $l$ | Length of the target | 3.0 cm |
| $\eta = 1.12\rho l N_A/M$ | Scatterers per area (Ref. 22) | $4.14\times10^{23}$ cm$^{-2}$ |
| $N_b\eta A^\alpha$ | Integrated luminosity | 1.10 pb$^{-1}$ |
| $f$ | Event-cut correction | 0.64 |
| $B(D^0\to\mu^+X)$ | $0.075\pm0.011\pm0.004$ | Ref. 23 |
| $B(D^+\to\mu^+X)$ | $0.170\pm0.019\pm0.007$ | Ref. 23 |
| $B(D^0\to K^-\pi^+)$ | $0.049\pm0.009\pm0.005$ | Ref. 24 |
| $B(D^{*0}\to D^0\pi^0)$ | $0.538\pm0.094$ | Ref. 25 |
| $B(D^{*0}\to D^0\gamma)$ | $0.462\pm0.094$ | Ref. 25 |
| $B(D^{*+}\to D^0\pi^+)$ | $0.489\pm0.083$ | Ref. 25 |
| $B(D^{*+}\to D^+\pi^0)$ | $0.340\pm0.070$ | Ref. 25 |
| $B(D^{*+}\to D^+\gamma)$ | $0.17\ \pm0.11$ | Ref. 25 |
| $B(\phi\to K^+K^-)$ | $0.493\pm0.010$ | Ref. 26 |
| $N(D^0)/N(D^+)$ | Number of $D^0$ per $D^+$ | 2.16 |
| $B_T$ | Average $D$-to-muon branching ratio | 0.105 |

TABLE II. The 95%-confidence upper limits on the $D\bar{D}$ production cross section determined from the right-sign $K\pi$ mass plot with consistent Cherenkov identification and $-0.7 \leq \cos(\theta_{\text{c.m.}}) < 0.7$ (Fig. 6). The column labeled $A_T$ contains the trigger-arm acceptances. The column labeled $A_F$ lists the corresponding forward-arm acceptances. The column labeled $\xi$ shows the fraction of the signal expected within the selected mass window. The sensitivity is the expected number of detected charmed particles per microbarn of $D\bar{D}$ production cross section.

$$B_F = B(D^0 \to K^- \pi^+) N(D^0)/[N(D^0)+N(D^+)] = 0.0335$$

| Model | $n$ | $b$ | $A_T$ | $A_F$ | $\xi$ | Sensitivity $(\mu\text{b})^{-1}$ | $\sigma$ Upper limit ($\mu$b) |
|---|---|---|---|---|---|---|---|
| Uncorrelated | 1 | 1.1 | 0.0104 | 0.143 | 0.79 | 5.7 | 51 |
| Uncorrelated | 3 | 1.1 | 0.0167 | 0.111 | 0.87 | 8.0 | 37 |
| Uncorrelated | 6 | 1.1 | 0.0232 | 0.088 | 0.92 | 9.3 | 32 |
| Correlated | 5 | 2.0 | 0.0287 | 0.085 | 0.96 | 11.6 | 26 |

of 2. The 95%-confidence upper limit on the $D\bar{D}$ cross section is given by the calculated cross section plus 1.645 times the upper uncertainty in that cross section. The uncertainty is determined by adding the statistical uncertainty in the number of excess combinations in quadrature with the systematic uncertainties in the integrated luminosity and the acceptances. The uncertainties due to the model assumptions and the branching ratios are not included. The statistical uncertainties in the acceptance calculations are negligible.

The 95%-confidence upper limits on the $D\bar{D}$ production cross section determined from the right-sign $K\pi$ mass plot using the consistent Cherenkov identification scheme and the $\cos(\theta_{\text{c.m.}})$ cut vary between 26 and 51 $\mu$b per nucleon for the production models employed (Table II). The level of hadronic production of charm reported in the literature at similar energies is on the order of tens of microbarns, indicating that this analysis is just short of being sensitive to the direct $K\pi$ decay mode of the $D$ meson.

### B. Cross sections from the charged-$D^*$ search

Interpreting the excesses observed in the right-sign mass difference plot and the corresponding $K\pi$ mass plot as $30\pm16$ charged-$D^*$ decays, and using the assumptions outlined previously, the $D\bar{D}$ production cross sections presented in Table III were obtained. The trigger-arm acceptance was calculated based upon a generated $D$-meson distribution, while the forward-arm acceptance was based upon $D^*$ production distributed according to the same model.[27] The dependence of the trigger-arm acceptance upon whether a $D$ or a $D^*$ is produced according to a given distribution is believed to be negligible.[28] The quoted systematic uncertainties include the uncertainty in the integrated luminosity and the acceptances, but exclude the effects of the model assumptions and the branching-ratio uncertainties.

Results from the prompt-electron-triggered experiment NA11 indicate that the $x_F$ dependence of $D^{*\pm}$ production fits to $n=3.2\pm1.5$ for the uncorrelated-production model.[29] Using the uncorrelated-production model with $n=3$ and $b=1.1$ $(\text{GeV}/c)^{-2}$, the charged-$D^*$ search presented here yields a $D\bar{D}$ production cross section of $34\pm18^{+14}_{-9}$ $\mu$b, which is compatible with the $D\bar{D}$ production cross sections reported from NA11.

### C. Upper limits on the ratio of $F$ to $D$ cross section

An upper limit on the ratio of the $F$ to $D$ cross section can be extracted from the data presented in Fig. 9 (combined with the results of the $D^*$ search). Assuming that the trigger-arm corrections are similar for the strange and nonstrange charmed mesons, and using the spin-weighted $D$ and $D^*$ production ratios, the ratio of the $F$ to $D$ cross section is given by

$$\frac{N_F \epsilon_{D^*} \frac{3}{8} B(D^{*+} \to D^0 \pi^+) B(D^0 \to K^- \pi^+)}{N_{D^*} \epsilon_F B(F \to \phi\pi) B(\phi \to K^+ K^-)} ,$$

where $N_F$ and $N_{D^*}$ are the number of excess combinations observed in the mass plots, $\epsilon_F$ and $\epsilon_{D^*}$ are the

TABLE III. $D\bar{D}$ production cross-section estimates based upon the charged-$D^*$ search illustrated in Fig. 7. The column labeled $A_F$ lists the forward-arm acceptances. The column labeled $\xi$ shows the fraction of the signal expected within the selected mass window.

$$B_F = B(D^{*+} \to D^0 \pi^+) B(D^0 \to K^- \pi^+) N(D^{*+})/[N(D^0)+N(D^+)] = 0.0090$$

| Model | $n$ | $b$ | $A_F$ | $\xi$ | Sensitivity $(\mu\text{b})^{-1}$ | $\sigma$ ($\mu$b) |
|---|---|---|---|---|---|---|
| Uncorrelated | 1 | 1.1 | 0.114 | 0.59 | 0.92 | $32\pm17^{+13}_{-8}$ |
| Uncorrelated | 3 | 1.1 | 0.061 | 0.66 | 0.89 | $34\pm18^{+14}_{-9}$ |
| Uncorrelated | 6 | 1.1 | 0.026 | 0.75 | 0.61 | $49\pm26^{+20}_{-13}$ |

TABLE IV. The 95%-confidence upper limit on the ratio of $F$ to $D$ cross section as a function of the branching ratio for $F\to\phi\pi$. The column labeled $A_F$ lists the forward-arm $F$ meson acceptances excluding the mass window requirement. The column labeled $\xi$ shows the fraction of the signal expected within the selected mass window.

| Model | $n$ | $b$ | $A_F$ | $\xi$ | $\sigma_F/\sigma_D$ Upper limit |
|---|---|---|---|---|---|
| Uncorrelated | 1 | 1.1 | 0.015 | 0.80 | $0.127/B(F\to\phi\pi)$ |
| Uncorrelated | 3 | 1.1 | 0.018 | 0.84 | $0.064/B(F\to\phi\pi)$ |
| Uncorrelated | 6 | 1.1 | 0.019 | 0.83 | $0.031/B(F\to\phi\pi)$ |

forward-arm acceptances, and the factor $\frac{3}{8}$ accounts for the charged $D^*$ relative to total $D$ production. The 95%-confidence upper limit on the ratio of the $F$ to $D$ inclusive cross sections are listed in Table IV subject to the additional assumption that $F$ and $D^*$ mesons are produced with the same $x_F$ and $p_T$ dependences. These upper limits are not very restrictive unless $B(F\to\phi\pi)$ is fairly large. In $e^+e^-$ experiments, the value of $B(F\to\phi\pi)$ has been estimated to be 0.044 (Ref. 14) and 0.13 (Ref. 15).

The $\phi\pi^\pm$ mass plot shown in Fig. 9 is only expected to contain about one Cabibbo-suppressed charged-$D$ decay. (Note that there is no right-sign for this decay mode.)

### D. Charm content of the prompt-muon-triggered events

Using the $D\bar{D}$ cross-section upper limits presented in Table II, the 95%-confidence upper limit on the fraction of DST events with triggering muons attributable to charmed sources is 40%. Using the $D\bar{D}$ cross section of $34\pm18$ $\mu$b determined from the charged-$D^*$ search, the fraction of the DST events with triggering muons that are due to charmed sources is $(30\pm16)$%.

The $D\bar{D}$ production cross section determined from the $D^{*\pm}$ search is $300\pm180$ $\mu$b per beryllium nucleus. The absorption cross section for $\pi^-$ on beryllium at 200 GeV/$c$ is 139 mb per nucleus.[30] Consequently $(0.21\pm0.13)$% of all interactions contained charmed particles. The prompt-muon trigger enhanced the fraction of recorded events containing charm to $(7.8\pm4.7)$%. The trigger combined with the off-line analysis enhanced the fraction of selected events containing charmed particles by about 2 orders of magnitude.

The excess opposite-sign $\mu e$ coincidences observed in this experiment indicated that 17% of the final event sample was from charmed sources. A study of the dimuons observed in the spectrometer indicated that 12% of the final event sample was triggered by muons from electromagnetic sources.[2] Pion and kaon decays were probably responsible for the majority of the remaining triggers in the final event sample.

### E. Conclusions

This experiment recorded prompt-muon-triggered data detected in a two-arm spectrometer to study the associated production and decay of charmed states produced by 205-GeV/$c$ $\pi^-$-beryllium interactions. The $D\bar{D}$ cross sections determined from this data indicated that about 20% of the events in the final sample were from charmed sources. Thus, the prompt-muon trigger coupled with the filtering analysis was effective in enhancing the charm content of the final data sample. The 95%-confidence upper limits on the $D\bar{D}$ production cross section inferred from an analysis of the right-sign $K^\mp\pi^\pm$ mass plots were between 26 and 51 $\mu$b per nucleon for the production models tested. Using the background suppression derived from the kinematics of the charged-$D^*$ decay into a neutral $D$ and a charged pion, an enhancement of $30\pm16$ combinations above background was observed in the $K\pi\pi$ final state with the expected trigger-muon charge. Interpreted as a charged-$D^*$ signal, this enhancement corresponds to a model-dependent inclusive $D\bar{D}$ production cross section of $34\pm18^{+14}_{-9}$ $\mu$b per nucleon. These results are in agreement with other measurements of the charm cross section at comparable energies.

## ACKNOWLEDGMENTS

We thank the Fermilab staff and the technical staffs of the participating universities for their support throughout this experiment. This research was supported by the U.S. Department of Energy and the National Science Foundation.

[a]Present address: University of Rochester, Rochester, NY 14627.
[b]Present address: Areté Associates, Arlington, VA.
[c]Present address: Fermilab, Batavia, IL 60510.
[d]Present address: 3M Company, St. Paul, MN 55144.
[e]Present address: Northwestern University, Evanston, IL 60201.
[f]Present address: University of Colorado, Boulder, CO 80302.
[g]Present address: Institute of High Energy Physics, P.O. Box 918-1, Beijing, China.
[h]Present address: The State University of New York at Stony Brook, Stony Brook, NY 11794.
[i]Present address: Hughes Aircraft Co., Los Angeles, CA 90009.

[j]Present address: University of Michigan—Flint, Flint, MI 48503.

[k]Present address: Dresser Atlas, Houston, TX 77042.

[1]A. Kernan and G. VanDalen, Phys. Rep. **106**, 297 (1984).

[2]R. M. Edelstein *et al.*, Phys. Rev. Lett. **53**, 1411 (1984). The cross section has been adjusted to reflect the semileptonic branching ratios and normalization employed in this paper.

[3]G. Coutrakon *et al.*, Fermilab Report No. Note FN-351, 1981 (unpublished).

[4]Additional details on the trigger-arm PWC construction and electronics are available in Lucien Marcus Cremaldi, Ph.D. thesis, Northwestern University, 1983 (unpublished).

[5]Additional details on the foward arm PWC's are available in J. Michael McQuade, Ph.D. thesis, Carnegie-Mellon University, 1983.

[6]Readout systems are described in detail in D. R. Green, Nucl. Instrum. Methods **158**, 249 (1979).

[7]W. Sakumoto *et al.*, Nucl. Instrum. Methods Phys. Res. **A235**, 61 (1985).

[8]Additional details on this analysis are available in George E. Ginther Jr., Ph.D. thesis, Carnegie-Mellon University, 1985.

[9]A track was in the discrimination domain of the Cherenkov counter if its momentum was between 7 and 20 GeV/$c$ and its light cone intercepted the active area of the Cherenkov counter.

[10]Willis Kazuo Sakumoto, Ph.D. thesis, Northwestern University, 1984.

[11]Upper limits on $D^0\overline{D}^0$ mixing have been reported, e.g., A. Bodek *et al.*, Phys. Lett. **113B**, 82 (1982), which quotes a 90%-confidence upper limit of 4.4% based on $D$ mesons decaying into wrong-sign muons. A model-independent 90%-confidence upper limit of 8.1% was determined from a study of charged-$D^*$ decays by H. Yamamoto *et al.*, Phys. Rev. Lett. **54**, 522 (1985).

[12]The uncertainty in the number of excess combinations resulted from the statistical uncertainty in the total number of combinations between 1.815 and 1.915 GeV/$c^2$ in quadrature with the uncertainty in the number of background combinations determined from the covariance matrix from the polynomial fit.

[13]This mass-difference-plot technique is a standard means of searching for the charged $D^*$; see e.g., V. L. Fitch *et al.*, Phys. Rev. Lett. **46**, 761 (1981).

[14]A. Chen *et al.*, Phys. Rev. Lett. **51**, 634 (1983).

[15]M. Althoff *et al.*, Phys. Lett. **136B**, 130 (1984).

[16]H. Aihara *et al.*, Phys. Rev. Lett. **53**, 2465 (1984); H. Albrecht *et al.*, Phys. Lett. **153B**, 343 (1985).

[17]R. Bailey *et al.*, Phys. Lett. **139B**, 320 (1984); A. Badertscher *et al.*, *ibid.* **123B**, 471 (1983).

[18]The $A$ dependence of $J/\psi$ production in a 200-GeV/$c$ $\pi^-$ beam is given by $A^\alpha$ where $\alpha=0.97\pm0.02$ according to J. Badier *et al.*, Z. Phys. C **20**, 101 (1983). However, the $A$ dependence of charm production is still an unsettled issue. For a recent discussion, see Jack L. Ritchie, in *Design and Utilization of the Superconducting Super Collider, Snowmass, 1984,* proceedings of the Snowmass Summer Study, edited by Rene Donaldson and Jorge G. Morfin (Fermilab, Batavia, IL, 1985), pp. 239 and 240.

[19]This assumption neglects contributions from the other charmed states that are stable against strong and electromagnetic decays. The $\Lambda_c(F)$ cross section for $x_F>0$ is less than 25% (6%) of the forward charm cross section based upon results reported by J. Hrubic, in *Proceedings of the XXII International Conference on High Energy Physics, Leipzig, 1984,* edited by A. Meyer and E. Wieczorek (Academic der Wissenschaften der DDR, Zeuthen, DDR, 1984), Vol. I, p. 159. Furthermore, the trigger-arm acceptance for muons from $\Lambda_c$ decays is smaller than for muons from $D$-meson decays due to the larger $Q$ of the $D$ decays, and the inclusive electronic branching ratio for $\Lambda_c$ decays is also smaller. Other upper limits on the hadronic production of $F$ mesons are reported in C. H. Georgiopoulos *et al.*, Phys. Lett. **152B**, 428 (1985) and M. Aguilar-Benitez *et al.*, *ibid.* **156B**, 444 (1985).

[20]M. Aguilar-Benitez *et al.*, Z. Phys. C **31**, 491 (1986).

[21]A study of the electron momentum spectrum from $D$ decays indicated that $37\pm16\%$ of the semileptonic $D$ decays proceed through $D\to K^*(890)e\nu$ and $55\pm14\%$ through $D\to Ke\nu$ as reported in W. Bacino *et al.*, Phys. Rev. Lett. **43**, 1073 (1979).

[22]Based upon a comparison of target-out and standard runs, a 12% increase in the calculated number of scattering centers was introduced to account for the materials in addition to the beryllium that served as target in this experiment.

[23]R. M. Baltrusaitis *et al.*, Phys. Rev. Lett. **54**, 1976 (1985).

[24]Rafe H. Schindler, in *Proceedings of the XXII International Conference on High Energy Physics, Leipzig, 1984* (Ref. 19), pp. 171—174.

[25]Particle Data Group, Errata for 1984 edition of "Review of Particle Properties," 1984 (unpublished).

[26]Particle Data Group, Rev. Mod. Phys. **56**, (1984).

[27]In calculating the forward-arm acceptance, the window applied to the mass-difference plot in the Monte Carlo simulation was from 0.144 to 0.147 GeV/$c^2$.

[28]The trigger-arm muon acceptances from $D$ and $D^*$ parents produced according to the uncorrelated model with $n=3$ and $b=1.1$ (GeV/$c$)$^{-2}$ were equal within the uncertainty due to the statistics of the study.

[29]R. Bailey *et al.*, Phys. Rev. **132B**, 230 (1983); **132B**, 237 (1983).

[30]A. S. Carroll *et al.*, Phys. Lett. **80B**, 319 (1979).